Improved Method for Estimating Precipitable Water Distribution using Numerical Prediction data

Shin Akatsuka[1*]

[1] School of Systems Engineering, Kochi University of Technology
185 Tosayamadacho-Miyanokuchi, Kami, Kochi, 782-8502, JAPAN

[*]E-mail: akatsuka.shin@kochi-tech.ac.jp

Abstract: The atmospheric water vapor is one of the greenhouse gasses that can lead to global warming. In addition, the atmospheric water vapor content is absolutely imperative for atmospheric correction, which is the most important part of the pre-processing of remote sensing data. Therefore, we need to grasp the atmospheric water vapor distribution for climate research and to mitigate atmospheric effects on remote sensing data. The author proposed the method for estimating precipitable water (PW) distribution at spatially higher resolution using numerical prediction data and digital elevation model (DEM) in Kanto region, Japan. However, the PW in lower-elevation region was underestimated by the method. In addition, the proposed method needed the coefficients, which were obtained after the monthly estimation of PW. Therefore, the method could not estimate PW distribution in near-real time after obtaining numerical prediction data. The purpose of this study is to improve estimation method for PW distribution using numerical prediction data and DEM. This study examined how to improve underestimation of PW in lower-elevation region, and to estimate PW distribution in near-real time after obtaining numerical prediction data. By conducting the elevation correction to the region, whose elevation is over 200 m, the overcorrection due to the elevation correction could be improved in lower -elevation region. This study compared the results of the accuracy evaluation between the MSM-refined PW estimation in 2016 using the elevation correction coefficients of 2016 and using the mean of elevation correction coefficients from 2010 to 2015. The difference between the results of accuracy evaluation was little, which was less than 0.05 mm in the mean of RMS difference, and 0.07 mm in the standard deviation of RMS difference. Therefore, by using the coefficients obtained from the monthly estimation of PW for former several years, the PW distribution can be estimated in near-real time after obtaining numerical prediction data.

Keywords: remote sensing, atmospheric correction, DEM

1. Introduction

The atmospheric water vapor is one of the greenhouse gasses that can lead to global warming. In addition, the atmospheric water vapor content is absolutely imperative for atmospheric correction, which is the most important part of the pre-processing of remote sensing data. Therefore, we need to grasp the atmospheric water vapor distribution for climate research and to mitigate atmospheric effects on remote sensing data. The author proposed the method

for estimating precipitable water (PW) distribution at spatially higher resolution using numerical prediction data and digital elevation model (DEM) in Kanto region, Japan[1]. However, the PW in lower-elevation region was underestimated by the method. In addition, the proposed method needed the coefficients, which were obtained after the monthly estimation of PW. Therefore, the method could not estimate PW distribution in near-real time after obtaining numerical prediction data[1].

The purpose of this study is to improve estimation method for the PW distribution using numerical prediction data and DEM. This study examined how to improve underestimation of PW in lower-elevation region, and to estimate PW distribution in near-real time after obtaining numerical prediction data.

2. Methodology

2.1 Data description

Mesoscale model (MSM) grid point value (GPV) data were used as numerical prediction data in this study. The spatial resolution of MSM GPV data is 5 km at the surface level and 10 km at each barometric surface; the corresponding time interval is 1 and 3 hour, respectively (Table 1). Reconstructed MSM GPV data, whose original data is the MSM GPV data from the Japan Meteorological Agency (JMA), are provided by the Research Institute for Sustainable Humanosphere (RISH) of Kyoto University in Japan. An archive data obtained by reconstructing the original MSM GPV data represents the most probable atmospheric state. This archive data comprises the initial value data obtained by the objective analysis and the predicted data using the forward initial value[6]. The MSM GPV data set from 2010 to 2016 were downloaded from RISH[6].

The Advanced Spaceborne Thermal Emission and

Reflection Radiometer (ASTER) Global Digital Elevation Model (GDEM) data was used as the DEM data. These data are generated using stereo-pair images collected by the ASTER instrument onboard Terra[4]. The original spatial resolution of ASTER GDEM data is approximately 30 m (1 arcsecond); in this study, the data were resampled to a spatial resolution of 90 m in order to reduce processing time. ASTER GDEM is shown in Fig. 1 as the base map.

Table 1. Description of MSM GPV data.

Variable	Level	Spatial resolution (km)	Time interval (h)
Air temperature (K)	Surface	5	1
Relative humidity (%)	Surface	5	1
Surface pressure (hPa)	Surface	5	1
Sea-level pressure (hPa)	Surface	5	1
Air temperature (K)	16 pressure levels*	10	3
Relative humidity (%)	16 pressure levels*	10	3

* 16 pressure levels: 1000, 975, 950, 925, 900, 850, 800, 700, 600, 500, 400, 300, 250, 200, 150, 100 hPa.
** 12 pressure levels: 1000, 975, 950, 925, 900, 850, 800, 700, 600, 500, 400, 300 hPa.

The PW values estimated from ground-based GPS data were used to validate the PW estimated from MSM GPV data. The PW at the GPS stations can be estimated from the travel-time delays of GPS signals between satellites and ground-based receivers if the temperature and pressure at the GPS stations are known[5]. According to previous studies[8,10], the GPS-derived PW at 3-h intervals were calculated from the

atmospheric delay data provided by the Geospatial Information Authority of Japan and the temperature and pressure at each GPS station interpolated from the observed values of JMA's Automated Metrological Data Acquisition Systems[1].
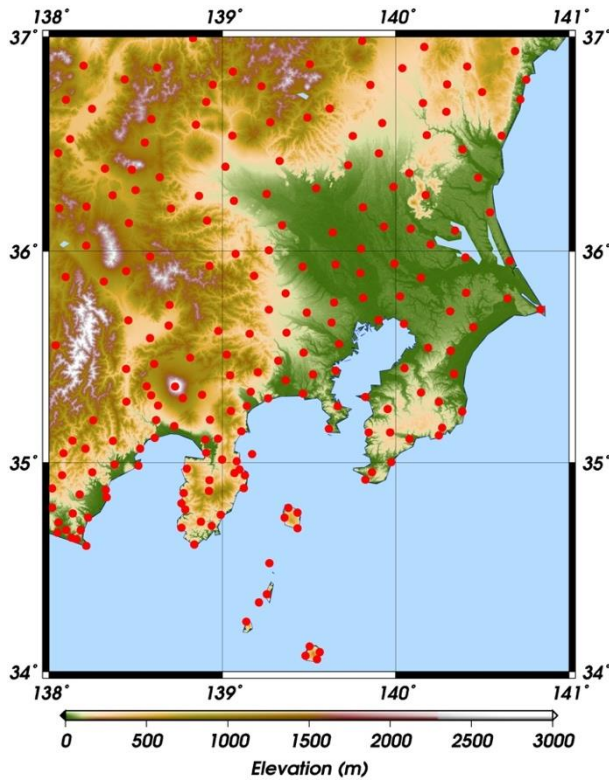

Fig.1. Locations of the study area along with GPS stations. The base map shows the elevation, which was mapped using ASTER GDEM data.

2.2 PW estimation from MSM GPV and DEM data

The PW distribution at a resolution of 5 km is calculated from MSM GPV data using Eq. (1) [1]:

$$IWV = \frac{100}{g}\left[\frac{q_s + q_{1000}}{2}(P_s - P_{1000})\right.$$
$$+ \frac{q_{1000} + q_{975}}{2}(P_{1000} - P_{975}) \quad (1)$$
$$\left. + \cdots + \frac{q_{400} + q_{300}}{2}(P_{400} - P_{300})\right]$$

where IWV is the integrated water vapor content between the surface and the 300 hPa barometric surface level (mm), P_s is the surface pressure (hPa), and q_s is the specific humidity (kgkg^{-1}) at the barometric surface level. In this study, the IWV between the surface and the 300 hPa barometric surface level is taken as PW.

The specific humidity at barometric level P_n can be calculated using Eq. (2):

$$q_n = \frac{0.622}{(P_n/e_{P_n}) - 0.378} \quad (2)$$

where q_n is the specific humidity (kg kg^{-1}) at barometric level P_n, and e_{P_n} is the water vapor pressure (hPa) at barometric level P_n.

The water vapor pressure at barometric level P_n can be calculated using Eq. (3):

$$e_{P_n} = \left(\frac{RH_{P_n}}{100}\right) \times e_{P_n,sat} \quad (3)$$

where e_{P_n} is the water vapor pressure (hPa) at barometric level P_n, RH_{P_n} is the relative humidity (%) at barometric level P_n, and $e_{P_n,sat}$ is the saturation water vapor pressure (hPa) at barometric level P_n.

The saturation water vapor pressure at barometric level P_n can be calculated using Eq. (4) [2]:

$$e_{P_n,sat} = 6.1094 \times exp\{17.625 T_{P_n}/(243.04 + T_{P_n})\} \quad (4)$$

where $e_{P_n,sat}$ is the saturation water vapor pressure (hPa) at barometric level P_n, and T_{P_n} is the air temperature (°C) at barometric level P_n.

MSM GPV data include the relative humidity and air temperature at 12 barometric levels (1000–300 hPa); thus, we can calculate integrated PW between the surface and the 300 hPa barometric level using Eqs. (1)–(4).

The PW distribution at 90-m resolution from MSM

GPV data can be estimated by accounting for the difference in surface elevation within grids of MSM GPV data using ASTER GDEM data with 90-m resolution[1].

Here, we focus only on a grid of MSM GPV data (G_{mn}) and a DEM pixel (D_{ij}) within G_{mn}. The PW of D_{ij} can be calculated from the specific humidity and surface pressure of D_{ij}, which can be estimated from both the MSM GPV and DEM data.

Assuming that air is an ideal gas and that the temperature lapse rate is 6.5 K km^{-1}, the elevation of G_{mn} ($H_{G_{mn}}$) can be calculated using the following relation[3,9]:

$$H_{G_{mn}} = \frac{T_{G_{mn}} + 273.15}{0.0065}\left\{\left(\frac{P_{SL,G_{mn}}}{P_{G_{mn}}}\right)^{1/5.257} - 1\right\} \quad (5)$$

where $T_{G_{mn}}$, $P_{G_{mn}}$, and $P_{SL,G_{mn}}$ are the surface air temperature (°C), surface pressure (hPa), and sea-level pressure of G_{mn} (hPa), respectively.

The surface pressure of D_{ij} ($P_{D_{ij}}$), whose elevation is $h_{D_{ij}}$ (m), can be expressed using $T_{G_{mn}}$, $P_{SL,G_{mn}}$, and $h_{D_{ij}}$ as[9]

$$P_{D_{ij}} = P_{SL,G_{mn}} \times \left(1 - \frac{0.0065h_{D_{ij}}}{T_{SL,G_{mn}} + 273.15}\right)^{5.257} \quad (6)$$

where $T_{SL,G_{mn}}$ is the sea-level air temperature (°C), which can be derived from Eq. (7) as

$$T_{SL,G_{mn}} = T_{G_{mn}} + 0.0065H_{G_{mn}} \quad (7)$$

The specific humidity of D_{ij} ($q_{D_{ij}}$) can be calculated from Eq. (8) as[7]

$$q_{D_{ij}} = \frac{0.622}{\left(P_{D_{ij}}/e_{D_{ij}}\right) - 0.378} \quad (8)$$

From Eqs. (3) and (4), the saturation water vapor pressure of D_{ij} ($e_{D_{ij}}$) can be calculated from Eq. (9) as

$$e_{D_{ij}} = \left(\frac{RH_{D_{ij}}}{100}\right) \times 6.1094 \\ \times exp\left\{17.625T_{D_{ij}}/\left(243.04 + T_{D_{ij}}\right)\right\} \quad (9)$$

where $T_{D_{ij}}$ is the sea-level air temperature (°C), which can be derived from Eq. (10):

$$T_{D_{ij}} = T_{SL,G_{mn}} - 0.0065h_{D_{ij}} \quad (10)$$

Finally, if $P_{D_{ij}} > 1000$ hPa, we assume that $RH_{D_{ij}} = RH_{G_{mn}}$, and the specific humidity of D_{ij} ($q_{D_{ij}}$) can then be estimated using Eqs. (6)–(10)[1]. If $P_{D_{ij}} \leq 1000$ hPa, we assume that $q_{D_{ij}} = q_{P_n,G_{mn}}$; $q_{P_n,G_{mn}}$ is the specific humidity of G_{mn} at barometric level P_n, which is the nearest barometric surface of $P_{D_{ij}}$[1].

For $P_{D_{ij}} > 1000$ hPa, the PW of D_{ij} can be estimated by Eq. (11)[1]:

$$PW_{D_{ij}} = \frac{100}{g}\left[\frac{q_{D_{ij}} + q_{1000}}{2}\left(P_{D_{ij}} - P_{1000}\right) \\ + \frac{q_{1000} + q_{975}}{2}(P_{1000} - P_{975}) \\ + \cdots \\ + \frac{q_{400} + q_{300}}{2}(P_{400} - P_{300})\right] \quad (11)$$

For $P_{D_{ij}} \leq 1000$ hPa, the PW of D_{ij} can be estimated by Eq. (12)[1]:

$$PW_{D_{ij}} = \frac{100}{g}\left[\frac{q_{P_n,G_{mn}} + q_{P_1}}{2}\left(P_{D_{ij}} - P_1\right) \\ + \frac{q_{P_1} + q_{P_2}}{2}(P_1 - P_2) + \cdots \\ + \frac{q_{400} + q_{300}}{2}(P_{400} - P_{300})\right] \quad (12)$$

$(P_2 < P_1 < P_{D_{ij}} \leq 1000)$

where P_1 is the nearest MSM GPV barometric surface from $P_{D_{ij}}$[1], and P_2 is the nearest MSM GPV barometric surface from P_1.

Because the atmospheric water vapor content decreases with increasing elevation[11,12], large

elevation differences between the MSM topography and the GPS stations may lead to larger biases. Therefore, the bias attributed to elevation difference should be removed via elevation correction to improve the accuracy of PW derived from MSM GPV and DEM[1].

The elevation correction can be formulated as follows[1]:

$$PW_{EC_m,D_{ij}} = PW_{D_{ij}} - a_m \times h_{D_{ij}} \qquad (13)$$

where $PW_{EC_m,D_{ij}}$ is the PW of D_{ij} after elevation correction, $PW_{D_{ij}}$ is the PW of D_{ij} without elevation correction, and a_m is the monthly slope of the linear regression between the biases and elevations of GPS stations, which is statistically significant (Table 2). In this method, it was assumed the slope to be constant within a given month.

Table 2. Monthly results of linear regression between the biases and elevations of GPS stations in 2014[1].

Month	Slope (a_m)	Intercept	R^2
Jan.	1.89×10^{-3} *	-0.43	0.53
Feb.	2.33×10^{-3} *	-0.09	0.63
Mar.	2.92×10^{-3} *	0.23	0.73
Apr.	3.73×10^{-3} *	0.09	0.80
May	5.65×10^{-3} *	-0.31	0.88
Jun.	8.97×10^{-3} *	0.12	0.90
Jul.	1.15×10^{-2} *	-0.25	0.93
Aug.	1.25×10^{-2} *	-0.70	0.95
Sep.	7.86×10^{-3} *	-0.24	0.89
Oct.	6.00×10^{-3} *	-0.32	0.86
Nov.	4.38×10^{-3} *	-0.47	0.83
Dec.	2.16×10^{-3} *	-0.66	0.57

*: p-value < 0.001.

According to the procedure, the 90-m-resolution PW was estimated at 3-h intervals using MSM GPV

and ASTER GDEM data by conducting elevation correction. From this point forward, we refer to this estimated PW as MSM-refined PW.

2.3 Improved Elevation Correction

In the explained method of Section 2.2, the root-mean-square (RMS) difference between extracted MSM-refined PW values of the pixels which include each GPS station and the corresponding GPS-derived PW values increased after elevation correction at some GPS stations located in the lower-elevation region. The bias between them at lower-elevation (less than approximately 200 m) GPS stations did not fit well to the regression line (Fig. 2). This means that the explained method could improve the RMS differences at GPS stations, whose elevation are over 200 m, but it became worse the RMS differences at GPS stations, whose elevation are under 200 m, due to the overcorrection of the PW.
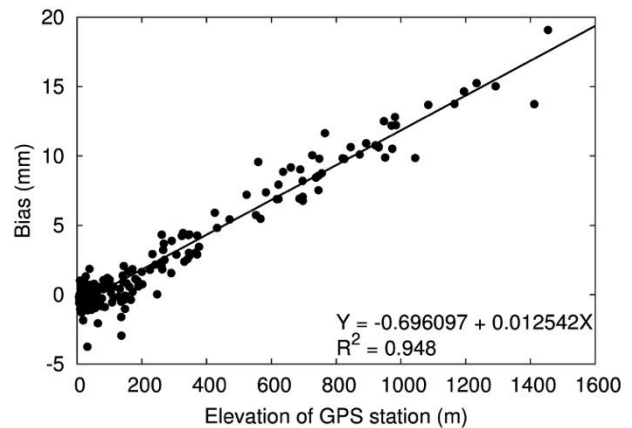

Fig. 2. Relationships between bias and elevation at GPS stations in August of 2014. The lines are linear regressions[1].

In this study, the elevation correction was conducted to the region, whose elevation is over 200 m, using the slopes and intercepts of linear regression between the biases and elevations of the GPS stations.

$$PW_{EC_m,D_{ij}} = PW_{D_{ij}} - \left(a_m \times h_{D_{ij}} + b_m\right)$$
$$(D_{ij} \geq 200) \tag{14}$$

where $PW_{EC_m,D_{ij}}$ is the PW of D_{ij} after elevation correction, $PW_{D_{ij}}$ is the PW of D_{ij} without elevation correction, and a_m, b_m is the monthly slope and intercept of the linear regression between the biases and elevations of GPS stations whose elevation are over 200 m, respectively.

2.4 Near-real time estimation

The method explained in Section 2.2 required the monthly estimation of PW to obtain the monthly coefficients for elevation correction. The monthly coefficients are obtained by the linear regression between the biases for each month and elevations of GPS stations. In other words, the monthly coefficients are obtained after the 3-hour interval PW were estimated using MSM GPV data for each month. Therefore, the method cannot estimate PW in near-real time after obtaining the 3-hour interval MSM GPV data.

In this study, we examined the influence of coefficients variation from year to year on the MSM-refined PW estimation in 2016 by comparing the results of the accuracy evaluation between the estimation using the mean coefficients from 2010 to 2015 and using the coefficients of 2016.

After the monthly coefficients for elevation correction were obtained from 2010 to 2015, the means of those coefficients were calculated. Then, for the accuracy evaluation, the means of the RMS difference between the GPS-derived PW and the MSM-refined PW in 2016 estimated by using the means of coefficients from 2010 to 2015 were calculated. Meanwhile, the means of the RMS difference between the GPS-derived PW and the MSM-refined PW in 2016 estimated by using the coefficients obtained after the monthly estimation of

PW in 2016 were calculated. If the difference between the results was little, by using the coefficients obtained from the monthly estimation of PW for former several years, the PW distribution can be estimated in near-real time after obtaining numerical prediction data.

3. Results and Discussion

3.1 Improved Elevation Correction

The both monthly slopes and intercepts of the linear regression between the biases and elevations of GPS stations whose elevation are over 200 m were calculated (Table 3).

Table 3. Monthly results of linear regression between the biases and elevations of GPS stations whose elevation are over 200 m in 2014.

Month	Slope (a_m)	Intercept (b_m)	R^2
Jan.	1.56×10^{-3} *	-0.15	0.46
Feb.	1.97×10^{-3} *	0.22	0.53
Mar.	2.60×10^{-3} *	0.51	0.67
Apr.	3.45×10^{-3} *	0.35	0.75
May	5.03×10^{-3} *	0.22	0.83
Jun.	7.82×10^{-3} *	1.07	0.79
Jul.	1.07×10^{-2} *	0.51	0.87
Aug.	1.25×10^{-2} *	-0.63	0.93
Sep.	7.12×10^{-2} *	0.41	0.80
Oct.	5.98×10^{-3} *	-0.26	0.79
Nov.	4.39×10^{-3} *	-0.44	0.79
Dec.	1.87×10^{-3} *	-0.40	0.48

*: p-value < 0.001.

According to the procedure explained in Section 2.2, the 90-m-resolution PW was estimated at 3-h intervals using the 2014 MSM GPV and ASTER GDEM data. Then, the improved elevation correction was conducted to the region, whose elevation is over 200 m, by using those values as the coefficients of elevation correction. We extracted the MSM-refined

PW values of the pixels which include each GPS station, and the monthly biases and RMS differences between extracted MSM-refined PW and the corresponding GPS-derived PW were calculated to evaluate the MSM-refined PW.

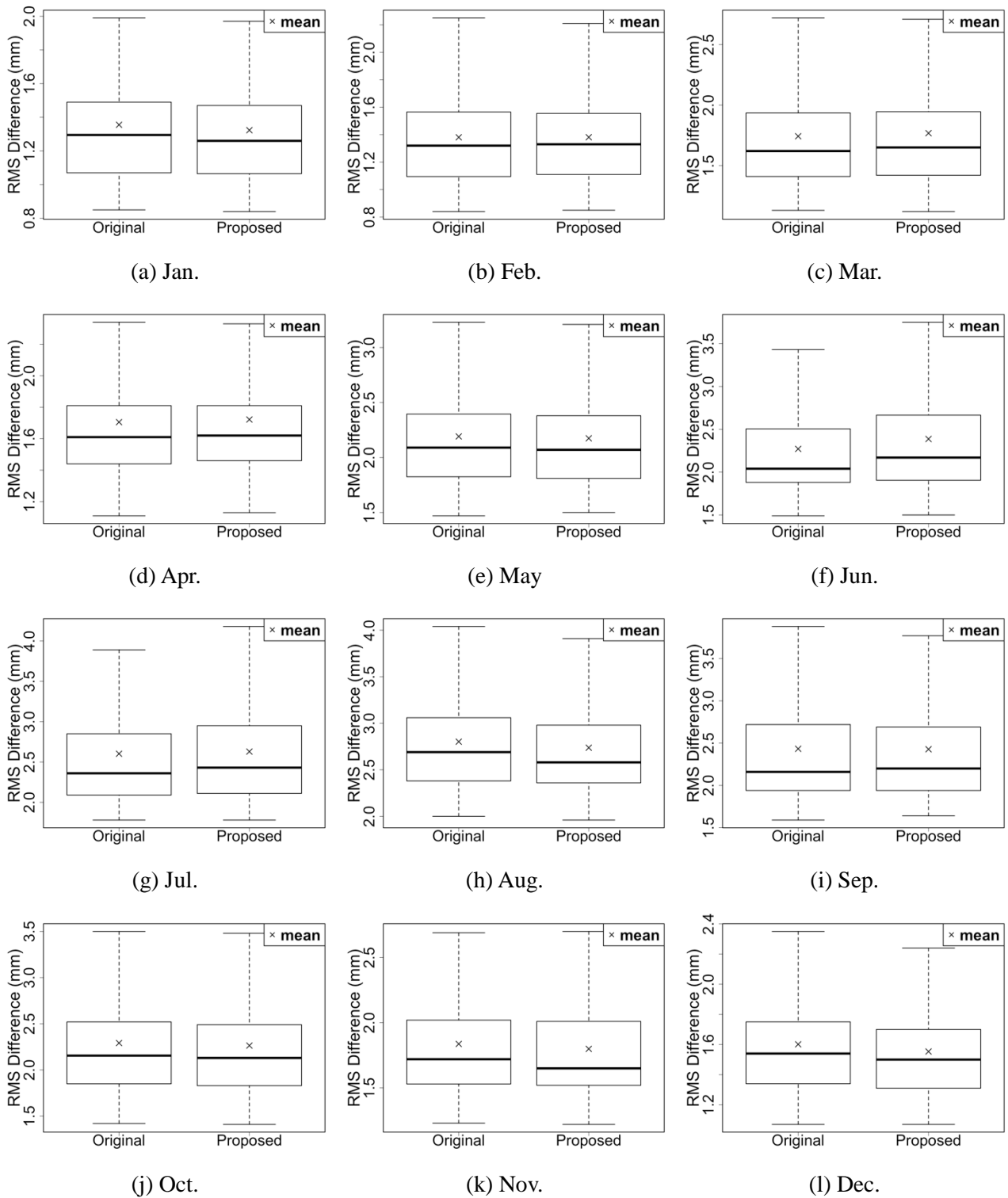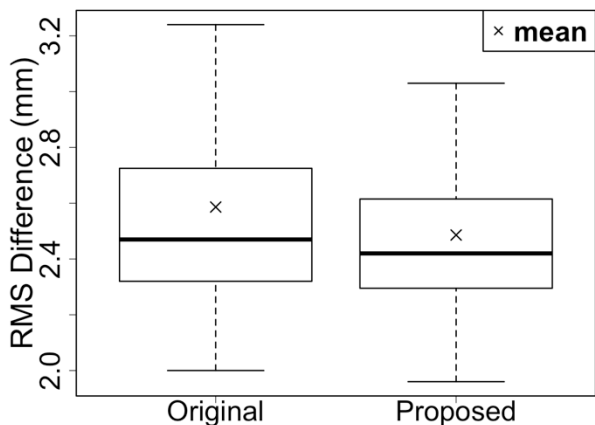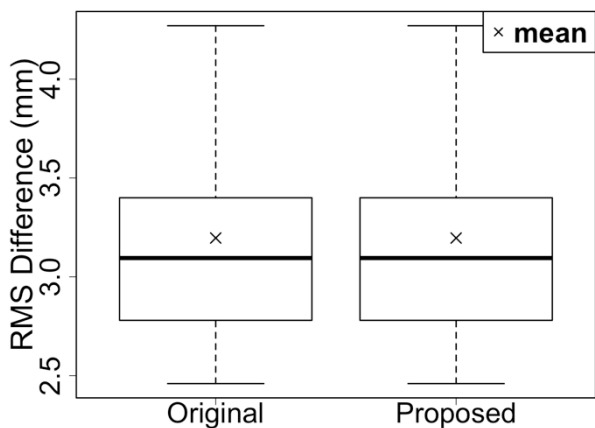| (a) Jan. | (b) Feb. | (c) Mar. |
(d) Apr.	(e) May	(f) Jun.
(g) Jul.	(h) Aug.	(i) Sep.
(j) Oct.	(k) Nov.	(l) Dec.

Fig. 3. The boxplot of the monthly mean of RMS difference in 2014 at each GPS station between the original method and the proposed method in this study.

(a) RMS difference at the GPS stations whose elevation is under 200 m.

(b) RMS difference at the GPS stations whose elevation is over 200 m.

Fig. 4. RMS difference in August of 2014 at each GPS station between the original method and the proposed method in this study.

Fig. 3 shows the monthly mean of RMS difference in 2014 at each GPS station between the original method and the proposed method in this study. As shown in Fig. 3, RMS difference became worse in March, June, and July. However, Fig.3 also indicated that the proposed method in this study slightly improved the RMS difference between MSM-refined PW and the GPS-derived PW in other months.

Fig. 4 shows the RMS differences in August of 2014 at each GPS station between the original method and the proposed method in this study. The original method could improve the RMS differences at GPS stations, whose elevation are over 200 m, but it

became worse the RMS differences at GPS stations, whose elevation are under 200 m, due to the overcorrection of the PW. Fig. 4 (a) shows the RMS differences at the GPS stations whose elevation are under 200 m, and Fig. 4 (b) shows the RMS differences at the GPS stations whose elevation are over 200 m. As shown in Fig. 4, the RMS differences at GPS stations, whose elevation are under 200 m, were improved by the proposed method in this study, and the RMS differences at GPS stations, whose elevation are over 200 m, did not become almost worse. This result means that the proposed method can improve the RMS differences at GPS stations, whose elevation are over 200 m, as same as original method, in addition it did not become worse the RMS differences at GPS stations, whose elevation are under 200 m.

3.2 Near-real time estimation

The monthly slopes and intercepts for elevation correction were obtained from 2010 to 2015 respectively, and then the means of those values were calculated. The 90-m-resolution PW was estimated at 3-h intervals using the 2016 MSM GPV and ASTER GDEM data. Then, MSM-refined PW of 2016 was calculated by conducting the elevation correction to the region, whose elevation is over 200 m, by using the mean values as the coefficients of elevation correction.

In addition, the monthly slopes and intercepts for elevation correction were obtained from 2016, and the 90-m-resolution PW was estimated at 3-h intervals using the 2016 MSM GPV and ASTER GDEM data. Then, MSM-refined PW of 2016 was calculated by conducting the elevation correction to the region, whose elevation is over 200 m, by using the values of 2016 as the coefficients of elevation correction.

Table 4 shows the mean values of the monthly

slopes (a_m) and intercepts (b_m) calculated from 2010 to 2015, and the values of the monthly slopes and intercepts obtained from only 2016.

Fig. 5 shows the mean of RMS difference at each GPS station in 2016. The circle symbol shows the result of MSM-refined PW estimation in 2016 by conducting the elevation correction using a_m and b_m (Table4), which are the mean values from 2010 to 2015, as the coefficients of elevation correction. The rectangle symbol shows the result of MSM-refined PW estimation in 2016 by conducting the elevation correction using a_m and b_m of 2016 as the coefficients of elevation correction (Table4). As shown in Fig. 5, when the mean values from 2010 to 2015 as the coefficients of elevation correction were used, the mean of RMS difference at each GPS station in August and September became slightly worse. In addition, in August and September, the standard deviation (S.D.) of RMS difference also became bigger than those derived from using the values of 2016 as the coefficients of elevation correction.

However, the degree of RMS difference degradation was very small throughout the year, which was less than 0.05mm in the mean of RMS difference, and 0.07 mm in the S.D. of RMS difference. Therefore, it was revealed that the estimation accuracy of MSM-refined PW did not become almost worse by using the coefficients obtained from the monthly estimation of PW for former several years. Thus, by using the coefficients obtained from the monthly estimation of PW for former several years, the PW distribution can be estimated in near-real time after obtaining numerical prediction data.

4. Conclusions

This study examined how to improve underestimation of PW in lower-elevation region, and the influence of coefficients variation from year to year on the MSM-refined PW estimation in 2016 by comparing the results of the accuracy evaluation between the estimation using the elevation correction coefficients of 2016 and using the mean of elevation correction coefficients from 2010 to 2015.

Table 4. Monthly results of linear regression between the biases and elevations of GPS stations.

| Month	Mean from 2010 to 2015		2016	
	Slope (a_m)	Intercept (b_m)	Slope (a_m)	Intercept (b_m)
Jan.	1.61×10^{-3}	-0.08	1.86×10^{-3} *	-0.22
Feb.	1.97×10^{-3}	-0.06	2.27×10^{-3} *	-0.38
Mar.	2.81×10^{-3}	0.01	3.03×10^{-3} *	-0.15
Apr.	4.29×10^{-3}	-0.01	4.90×10^{-3} *	-0.17
May	5.53×10^{-3}	0.09	6.16×10^{-3} *	-0.33
Jun.	8.14×10^{-3}	0.36	8.58×10^{-3} *	0.11
Jul.	1.10×10^{-2}	0.21	1.07×10^{-2} *	0.43
Aug.	1.15×10^{-2}	0.15	1.13×10^{-2} *	1.17
Sep.	9.21×10^{-3}	-0.26	1.11×10^{-2} *	-0.66
Oct.	6.12×10^{-3}	-0.30	6.50×10^{-3} *	-0.50
Nov.	4.01×10^{-3}	-0.23	3.84×10^{-3} *	-0.28
Dec.	2.27×10^{-3}	-0.18	2.42×10^{-3} *	-0.34

*: p-value < 0.001.
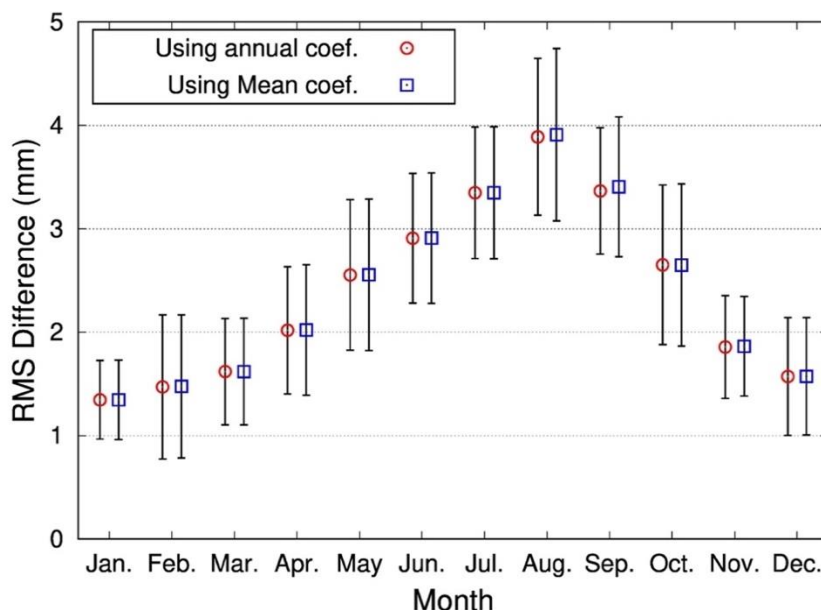
Fig. 5. The mean of RMS difference at each GPS station in 2016. The error bar represents one standard deviation. The circle symbol shows the result using the mean values of slopes and intercepts from 2010 to 2015 as the coefficients of elevation correction. The rectangle symbol shows the result using the values of slopes and intercepts of 2016 as the coefficients of elevation correction.

By conducting the elevation correction to the region, whose elevation is over 200 m, the RMS difference in lower-elevation region could be prevented from becoming worse due to the overcorrection of the elevation correction.

This study compared the results of the accuracy evaluation between the MSM-refined PW estimation in 2016 using the elevation correction coefficients of 2016 and using the mean of elevation correction coefficients from 2010 to 2015. The difference between the results of accuracy evaluation was little throughout the year, which was less than 0.05mm in the mean of RMS difference, and 0.07 mm in the S.D. of RMS difference. Therefore, it was revealed that by using the coefficients obtained from the monthly estimation of PW for former several years, the PW distribution can be estimated in near-real time after obtaining numerical prediction data.

References

1) Akastuka, S., Susaki J. and Takagi M., 2018. "Estimation of precipitable water using numerical prediction data," *Engineering Journal*. 22(3):257-268.

2) Alduchov O. A., and Eskridge R. E., 1996. "Improved Magnus form approximation of saturation vapor pressure," *J. Appl. Meteorol.*, 35(4):601-609.

3) Jan S., Gebre-Egziabher D. and Walter T., 2008. "Improving GPS-based landing system performance using an empirical barometric altimeter confidence bound," *IEEE. Trans. Aerosp. Electron. Syst..*, 44(1): 127-146.

4) Jet Propulsion laboratory, NASA. 2017, ASTER Global Digital Elevation Map Announcement. URL: https://asterweb.jpl.nasa.gov/gdem.asp (last date accessed: 24 July 2019)

5) Means J. D., 2013. "GPS precipitable water as diagnostic of the North American monsoon in California and Nevada," *J. Climate*, 26(4):1432-1444.

6) Research Institute for Sustainable Humanosphere, Kyoto University. 2017, Data form Japan Meteorological Agency.
URL: http://database.rish.kyoto-u.ac.jp/arch/jmadata/ (last date accessed: 24 July 2019)

7) Ross R. J. and Elliott W. P., 1996. "Tropospheric water vapor climatology and trends over North America: 1973-93," *J. Climat*e, 9(12):3561-3574.

8) Vey S., Dietrich R., Rülke A. and Fritsche M., 2010. "Validation of precipitable water vapor within the NCEP/DOE reanalysis using global GPS observation from one decade," *J. Climate*, 23(7):1675-1695.

9) Sakai T., Koremura K. and Niimi K., 2005. "Height measurement error of barometric altimeter and its correction," *ENRI Papers*, 114: 1-13.

10) Shangguan M., Heise S., Bender M., Dick G., Ramatschi M. and Wickert J., 2015. "Validation of GPS atmospheric water vapor with WVR data in satellite tracking mode," *Ann. Geophys*., 33(1):55-61.

11) Shuanggen J., Li Z. and Cho J., 2008. "Integrated water vapor field and multiscale variations over China from GPS measurements," *J. Appl. Meteor. Clim.*, 47(11):3008-3015.

12) Wang H., Wei M., Li G., Zhou S. and Zeng Q., 2013. "Analysis of precipitable water vapor from GPS measurements in Chengdu region: Distribution and evolution characteristics in autumn," *Adv. Space Res*, 52(4):656-667.